Modeling Identification and Control of Peltier Thermoelectic Modules for Telepresence

Mohamed Guiatni
Control Laboratory,
Military Polytechnics Institute,
Algiers 16111, Algeria
e-mail: mohamed.guiatni@gmail.com

Abderrahmane Kheddar
Joint Robotics Laboratory (JRL),
CNRS-AIST UMI3218/CRT,
Tsukuba 305-8568, Japan;
Laboratoire d'Informatique de Robotique et de
Microélectronique de Montpellier (LIRMM),
CNRS-UM2 UMR5506,
CC 477, 34095 Montpellier Cedex 5, France
e-mail: kheddar@lirmm.fr

This research deals with thermal rendering for telepresence applications. We present the modeling and identification of thermo-electric modules (TEMs) to be used either as part of a thermal display or a remote thermal probe. First, TEMs are modeled in steady- and unsteady-state dynamics using recursive nonlinear autoregressive moving average models for both temperature and heat flux. The proposed models are convenient for simulation, control, electronic, and thermal engineering. They allow understanding the functionality of the heat pumps and facilitate the solving of cooling/heating problems without the need for expertise in thermal theory. Then, these models are used in a novel thermal rendering approach that is based on the estimation of the temperature in contact for both the finger and the probed remote object in a telepresence setup. The thermal feedback is provided by a bilateral control between the master (thermal display) and the slave (thermal probe robotic finger). Experimental results validating the models and the proposed thermal rendering scheme are presented and discussed. [DOI: 10.1115/1.4003381]

1 Introduction

The thermal sensation, permeating and accompanying our tactual impressions, influences considerably our capability to distinguish several objects in our surrounding world by the simple act of touch. Yet, human perception of thermal stimuli is still not well/totally understood. The state-of-the-art regarding thermal perception and display has been recently described in Ref. [1]. Thermal displays consist generally of a heat source, a Peltier pump, or a power heater, and the control uses simple proportional-integral-derivative (PID) regulator that reproduces premeasured and precomputed temperature profiles on a thermal pad in contact with the human finger [2–4].

Recent approaches in haptics use the physiological composition of the human finger (bone, blood, and skin) and thermo-electric laws to model the heat exchange occurring in fingertip when touching an object. The authors in Ref. [5] present a model for the heat transfer occurring between the finger and a material and use it for computing a thermal feedback model in virtual reality. In Ref. [6], thermal rendering is based on contact temperature prediction and finger effusivity measurement. In Ref. [7], the heat conduction between skin and object is modeled by ordinary differential equations. Three different layers of tissue (epidermis, dermis, and endodermis) are distinguished within the finger. The work of Ho and Jones [8] proposes a prediction model for contact heat flux and temperature based on an infrared camera during interaction phases. An infrared thermal measurement system is also designed in Ref. [9] so that it can be used to evaluate the performance of a thermal display. This measurement system requires that the contact material be transparent in both the infrared and visible spectra. It is therefore designed so that skin temperature can be measured more accurately during contact, but not as a system that would be integrated into a haptic interface. In Ref. [10], an artificial finger is developed for research in car industry. This device is used to reproduce the human thermal rendering of interior parts in cars by means of synthetic materials having thermal properties nearly similar to that of the human finger.

Most of the thermal feedback methods presented previously cannot produce satisfactory thermal sensations when used in a telepresence where the operator and the material are not in direct contact. An exception is the work presented in Ref. [11] where the thermal feedback is based on a bilateral coupling scheme between the heat flux and the temperature using a four channel scheme.

In our previous works, we proposed a new model of thermal rendering for virtual reality applications in Ref. [12]. Yet, in its original form, our model cannot apply to telepresence. We have also proposed thermal rendering based on machine learning in Ref. [13]; it is based on thermal heat flux generation using two databases constructed from real measurements recorded during direct contact between the operator's finger and different candidate materials. Yet, this record/replay method produces latencies in flux and temperature profiles, which are due to the time needed for material recognition at first contacts.

In this work, thermal feedback is based on a new bilateral control scheme, which couples the thermal display (master) with the thermal remote probe, e.g., a robotic thermal finger (slave). The temperature evolution of each element of the coupled system is modeled and identified. The nonlinear models of the thermo-electric module (TEM) are used to estimate the interaction temperature of the operator finger (in contact with the thermal display) and that of the remote object (in contact with the thermal probe). In the proposed control scheme, the slave device is asked to track the estimated temperature of the operator finger, while the master device is asked to track the estimated temperature of the remote object. The material interface that is developed is used for thermal rendering and thermal identification of the remote touched/probed object.

2 Modeling the Thermo-Electric Module

A TEM (usually named Peltier pump) consists of multiple semiconductor junctions connected in series electrically and in parallel thermally between two plates (Fig. 1). The plates must be both good conductors of heat and good electrical insulators. Ceramic materials fulfill this particular property: One plate is thermally connected to a radiator, and the other to the object whose temperature is to be controlled. Thanks to the Peltier physical effect, a current through the junctions creates a temperature difference between the plates whose polarity and magnitude depend on those of the current. Relative to the ambient temperature, it thus becomes possible to heat the object or cool it down (via one TEM

Contributed by the Dynamic Systems Division of ASME for publication in the Journal of Dynamic Systems, Measurement, and Control. Manuscript received September 1, 2009; final manuscript received December 23, 2010; published online March 25, 2011. Assoc. Editor: Ahmet S. Yigit.

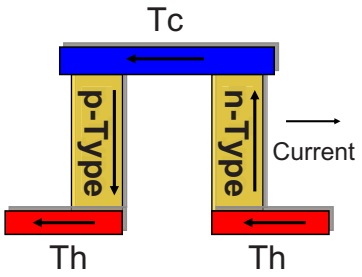

Fig. 1 Construction of a Peltier semiconductor element. In practice, several elements are generally connected in series electrically and in parallel thermally (T_h denotes the temperature of the hot side and T_c denotes the temperature of the cold side).

plate). Today's technology allows single-module temperature differences as high as 84°C, and cascading arrangements can produce even higher differences.

TEMs are widely used today in many applications, from thermal stabilization to microrefrigeration. TEMs can be used where cooling or temperature control of an object is required. Generally, TEMs are most often used

1. in applications where an object needs to be cooled below the ambient temperature or needs to be maintained at a constant temperature [14–17] and
2. as a thermal-haptic display for virtual reality and telepresence systems [11,5,18]. Precisely, in this case, we need to control the TEM in order to get fast and exact response both in temperature and in heat flux.

The difficulty resides in writing reliable explicit mathematical models that relate the input current, driving the TEM, to the temperature of each side of the TEM. These equations are hard to determine and a precise analysis of the electrothermal Peltier effect is difficult; this is because of the nonlinear behavior of the TEM that acts as a floating load for the voltage supply and the several phenomena that occur within it. Several numerical models have been proposed in the literature. Most of them are discrete finite element model (FEM) or finite difference model (FDM) [19–21].

In Ref. [22], a Simulation Program with Integrated Circuit Emphasis (SPICE) compatible equivalent circuit of TEM is proposed; it is convenient for electronic engineers. Indeed, representing the problem in electronic circuit language facilitates the solving of cooling/heating problems without the need for expertise in thermal theory. In Ref. [23], it is shown that the characteristics of a thermo-electric device can be described with a second-order discrete time autoregressive moving average (ARMA) model. The parameters of such a model vary with the operating point that is defined by the bias excitation current.

We propose a more refined, yet simple, model for TEMs that avoids complex modeling methods; it is a nonlinear dynamic representation based on a nonlinear ARMA model for temperature control that accounts for nonlinearities that are not considered in Ref. [23]. We also propose a model for solving steady-state cooling/heating capacity and a model describing the temperature/heat flow relation. These models are then used in the control laws that achieve thermal telepresence.

2.1 Thermophysical Models. When the electric current flows through a circuit composed of junctions between *n*- and *p*-type semiconductors (see Fig. 1), heat is liberated at one junction and absorbed by the other one depending on the direction in which the current is flowing: This is the Peltier effect. The quantity of heat P liberated per unit of time is proportional to the current [24,25]:

$$\frac{dE}{dt} = P_p = \pi I = \alpha_s T I \tag{1}$$

where π (V) is the Peltier coefficient, α_s (V K^{-1}) is the Seebeck coefficient, T (K) is the absolute temperature, and I (A) is the electric current. If an electric current flows in a homogeneous conductor in the direction of a temperature gradient dT/dx, heat will be absorbed or given out depending on the material: This is the Thomson effect,

$$P_t = \tau I \frac{dT}{dx} \tag{2}$$

where τ (V K^{-1}) is the Thomson coefficient and x (m) is the space variable. The direction in which the heat flows depends on the sign of the Thomson coefficient, the direction in which the current flows, and the direction of the temperature gradient.

On the other hand, heat is also generated due to the Joule effect, which is assumed uniformly distributed throughout the conductor. If an electric current I flows in an isothermal conductor of resistance R, the Joule effect is written as

$$P_j = RI^2 \tag{3}$$

Because of heat conduction, heat also flows from the hot side (temperature T_h) to the cold side (temperature T_c), hence

$$P_k = K(T_h - T_c) \tag{4}$$

where K is the thermal conductance. The steady-state cooling capacity of the pump on the cold side is

$$P_c = n\left\{\alpha T_c I \pm \frac{\tau I(T_h - T_c)}{2e} - \frac{1}{2}RI^2 - K(T_h - T_c)\right\} \tag{5}$$

where e is the thickness of the Peltier component and n is the number of components. The steady-state heating capacity of the pump on the hot side is

$$P_h = n\left\{\alpha T_h I \pm \frac{\tau I(T_h - T_c)}{2e} + \frac{1}{2}RI^2 - K(T_h - T_c)\right\} \tag{6}$$

A common convention in the thermoelectricity literature shows that half of the Joule and Thomson heats generated within a thermocouple is transferred to its heated side and the other half of it to its cooled side and the temperature distribution in the pellets is symmetric about their midpoints [26,27].

The plus-minus sign in Eqs. (5) and (6) means that the Thomson effect may be positive or negative: In the positive Thomson effect, it is found that the hot end is at high potential and the cold end is at low potential. Heat is evolved when current is passed from the hotter end to the colder end and heat is absorbed when current is passed from the colder end to the hotter end. Whereas in the elements showing negative Thomson effect, it is found that the hot end is at low potential and the cold end is at higher potential. Heat is evolved when current is passed from the colder end to the hotter end and heat is absorbed when current flows from the hotter end to the colder end.

Equations (5) and (6) represent the steady-state behavior of the TEM; similar models can be found in Refs. [28,27,29–31]. The description of transient behavior is more complex, but it is required in real-time simulation and controller synthesis for thermal rendering, which perception relies on first instants of contact.

2.2 Proposed Models. Based on the previous steady-state models, we assume that the dynamic behavior of the TEM can be correctly described by the following discrete-time ARMA model [23]:

$$T(t) = -\sum_{i=1}^{n} a_i T(t-i) + \sum_{j=0}^{m} b_j I(t-j) \tag{7}$$

where a_i and b_j are parameters depending on the current $I(t)$ and n and m represent the model's order according to T and I, respec-

tively. They are chosen to make a trade-off between the complexity of the model and its efficiency.

We propose recursive polynomial functions to describe the dependence of the parameters on current [32]. That is,

$$a_i = \sum_{k=0}^{p} a_{ik} I(t-i)^k \tag{8}$$

$$b_j = \sum_{h=0}^{q} b_{jh} I(t-j)^h \tag{9}$$

where p and q represent the polynomial order according to a and b, respectively. They are also chosen to make a trade-off between the complexity of the model and its efficiency. The complete description leads to the nonlinear ARMA model:

$$T(t) = -\sum_{i=1}^{n}\sum_{k=0}^{p} a_{ik} I(t-i)^k T(t-i) + \sum_{j=1}^{m}\sum_{h=0}^{q} b_{jh} I(t-j)^h I(t-j) \tag{10}$$

which is a linear model of the unknown parameters θ:

$$T(t) = \theta^T \varphi(t) \tag{11}$$

where

$$\theta = [a_{ik}, \{i = 1 \cdots n,\ k = 0 \cdots p\};\ b_{jh}, \{j = 0 \cdots m,\ h = 0 \cdots q\}]$$

is the vector of parameters of dimension $d = n(p+1) + m(q+1)$ and

$$\varphi(t) = [I(t-i)^k T(t-i),\ \{i = 1 \cdots n,\ k = 0 \cdots p\};\ I(t-j)^{h+1},\ \{j = 0 \cdots m,\ h = 0 \cdots q\}]$$

is the regression vector of dimension d. This model is particularly useful for temperature control. However, in our application, it is used to estimate the TEM's temperature evolution when this latter is in contact with an operator's fingertip or an object. For the relation between the temperature T and the heat flux Q, we also proposed an ARMA model:

$$Q(t) = -\sum_{i=1}^{n} c_i Q(t-i) + \sum_{j=0}^{m} d_j T(t-j) \tag{12}$$

where $c_i\ \{i = 1 \cdots n\}$ and $d_j\ \{j = 0 \cdots m\}$ are the model parameters to be identified. This model represents the thermal impedance of the TEM. It can be used to control the impedance of the TEM when used as a thermal display. In this case, impedance control can give a better trade-off between the temperature control and the heat flux control schemes [11].

3 TEM Model Identification

3.1 Experimental Setup. Figure 2 shows thermal telepresence setup. The master and the slave parts consist of a contact pad using one TEM from MELCOR Corp.™ (Trenton, NJ) with a dimension of $15 \times 15 \times 3.2$ mm^3. Each TEM is in thermal contact on one side with a heat sink with high thermal conductivity and on the other side with the heat flux sensor with a sensibility of 1.24 μV/W/m^2 and which incorporates a T-type thermocouple.

From a performance standpoint, a thermocouple measurement is stable over time. Also, computing the temperature from the thermocouple voltage is a straightforward one-step calculation, making it simple.

With heat flux measurements, having a good thermal contact between the heat flux sensor and the surrounding material is critical to achieving this goal. Without good thermal contact, the heat flow is disrupted. This causes some heat to flow around the sensor instead of through it, biasing the measurement. Eliminating air gaps around the sensor is the most common precaution that must be taken to maintain good thermal contact. Therefore, silicone grease is used to decrease the contact resistance at the contact surface of the TEM. The ambient temperature is measured using an infrared thermal sensor in order to compensate the initial temperature of the thermocouple and its environment.

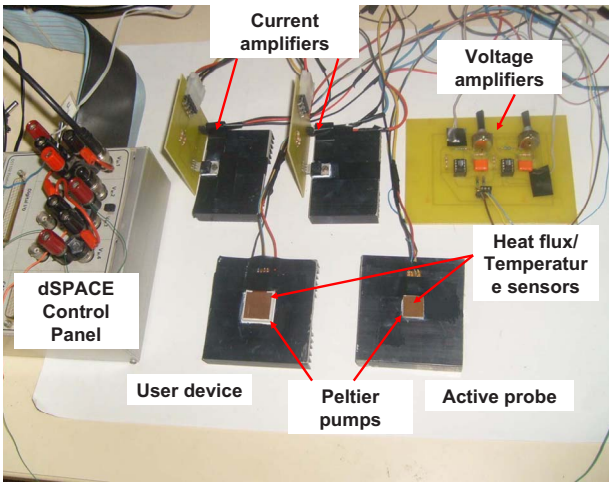

Fig. 2 Master/slave thermal telepresence setup

Current amplifiers are used for driving the TEMs. Voltage amplifiers are used for the flux/temperature sensor signals; sensors measure the current provided to each device. In order to reduce the sensors' sensibility to noise, the measured temperature and heat flux signals are filtered using a second-order low-pass digital filter. The whole system is controlled in real time via a Digital Processing and Control Engineering[1] dSPACE control setup.

3.2 Identification of the Heating/Cooling Capacity Models. Equations (5) and (6) can also be rewritten as

$$\begin{cases} P_c = \theta_{c1} T_c I + \theta_{c2} I^2 + \theta_{c3} T_c + \theta_{c4} I + \theta_{c5} = \theta_c^T \varphi_c \\ P_h = \theta_{h1} T_h I + \theta_{h2} I^2 + \theta_{h3} T_h + \theta_{h4} I + \theta_{h5} = \theta_h^T \varphi_h \end{cases} \tag{13}$$

with

$$\varphi_{h,c} = [T_{h,c} I, I^2, T_{h,c}, I, 1]^T$$

being the measure vectors and $\theta_{h,c}$ the unknown vectors.

Models given by Eqs. (5) and (6) are linear functions of the parameters to be estimated. We propose a similar form for the model to be estimated:

$$\{\hat{P}_{h,c} = \hat{\theta}_{h,c}^T \varphi_{h,c} \tag{14}$$

In this experiment, we measured both the steady-state temperature and the heat flux (when the equilibrium is reached) for $N = 14$ different current values chosen in the interval [−1.5 A, +1.5 A]. This has led to a set of triplets (current, temperature, and heat flux) reflecting the steady-state behavior of the device. The elements of the vectors $\theta_{h,c}$ can be determined by solving the following parameter optimization problem:

$$\hat{\theta}_{h,c} = \arg\min_{\theta_{h,c}} \left\{ \sum_{t=1}^{N} [P_{h,c}(t) - \hat{P}_{h,c}(t)]^2 \right\} \tag{15}$$

where N denotes the length of the measurement vectors. Using the linear least square method (LSM), we have

$$\{\hat{\theta}_{h,c} = (\Phi_{h,c}^T \Phi_{h,c})^{-1} \Phi_{h,c}^T P_{h,c} \tag{16}$$

where

[1] url: www.dspace.com

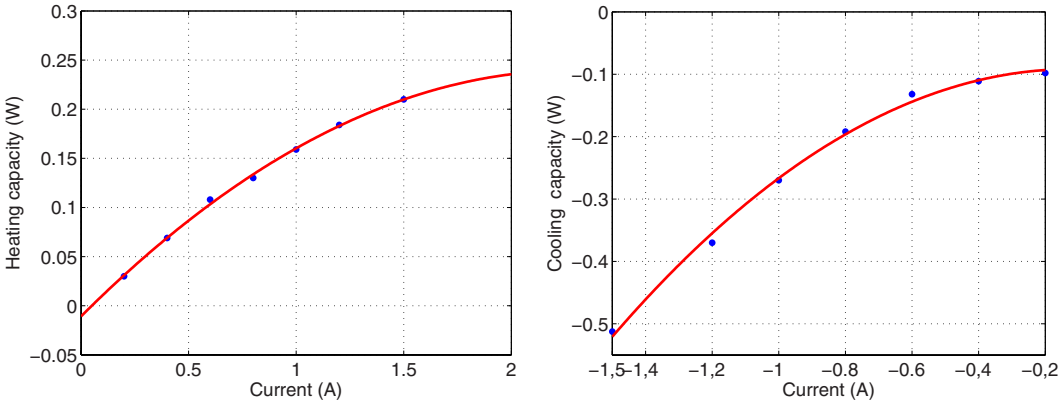

Fig. 3 Estimated (line) and measured (points) heating capacities (left) and estimated (line) and measured (points) cooling capacities (right)

$$\Phi_{h,c} = [\varphi_{h,c}(i),\ \ i = 1 \cdots N]$$

are measurement matrices. The estimated cooling/heating capacity by the identified model matches the real measurement (see Fig. 3). The values of the estimated parameters are given in Ref. [32]. Applications of the proposed model for cooling/heating capacities concern generally the performance analysis of the TEMs to be used, for example, for cooling microelectronic integrated circuits or for domestic refrigeration.

3.3 Identification of the Temperature Dynamic Model. A pseudorandom binary sequence (PRBS) signal approximating a white noise signal with variable amplitude sampled at 0.01 s is used as an input. The same experiment is realized with the two TEMs. The parameters of the model equation (10) are determined by solving the following parameter optimization problem:

$$\hat{\theta}_{LS} = \arg\min_{\theta}\left\{\sum_{t=n}^{M}[T(t) - \hat{T}(t)]^2\right\} \tag{17}$$

where $\hat{\theta}_{LS}$ and $\hat{T}$ are the estimated parameters and the temperature, respectively, and $M = 10{,}000$. The LSM algorithm is also used,

$$\hat{\theta}_{LS} = (\Phi^T\Phi)^{-1}\Phi^T Y$$

where $Y = \{T(t), t = n \cdots M\}$.

The above parameter optimization problem is improved by using the recursive least square method (RLSM):

$$\hat{\theta}(t) = \hat{\theta}(t-1) + K(t-1)\varphi(t)\varepsilon(t)$$

where $\hat{\theta}(t)$ is the estimated vector at t, $K(t)$ is the Kalman matrix gain, and ε is the estimation error defined as

$$\varepsilon(t) = \frac{y(t) - \theta(t-1)\varphi(t)}{1 + \varphi(t)^T K(t-1)\varphi(t)}$$

The Kalman gain update is computed as follows:

$$K(t) = \frac{1}{\lambda_1}\left[K(t-1) - \frac{K(t-1)\varphi(t)\varphi(t)^T K(t-1)}{\frac{\lambda_1}{\lambda_2} + \varphi(t)^T K(t-1)\varphi(t)}\right]$$

where λ_1 and λ_2 are the forget factors and $K(0)$ is the initial matrix gain (influences the convergence properties of the algorithm).

Figure 4 illustrates the measured TEM temperature compared with the estimated temperature; the identified model is for $n = p = m = q = 3$ (best trade-off between the complexity and efficiency). In the worst case, the error between real and estimated temperatures reached 0.3 °C. The estimated parameters are given in Ref. [32].

3.4 Identification of the Temperature/Heat Flux Dynamic Model. The measurement sequences performed in the previous section are also used for the identification of the parameters of the

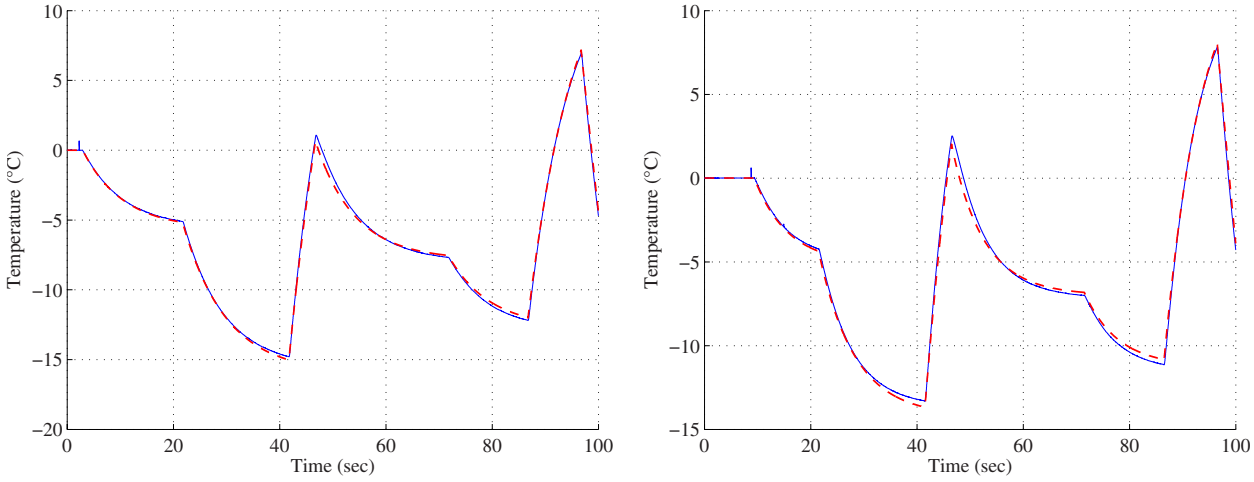

Fig. 4 Estimated (dashed) and measured (solid) temperatures of TEMs I (left) and II (right)

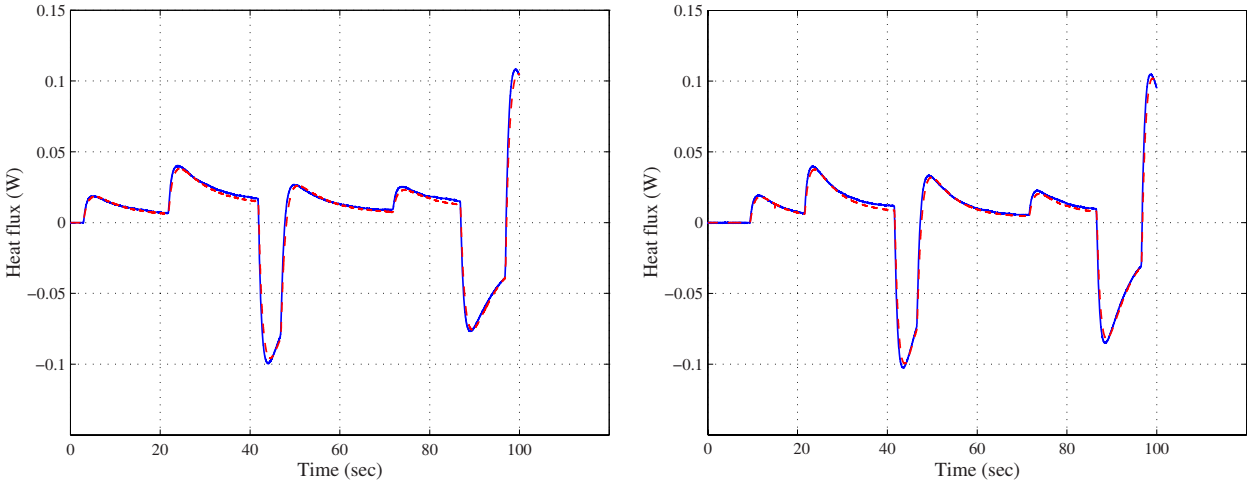

Fig. 5 Estimated (dashed) and measured (solid) heat fluxes of TEMs I (left) and II (right)

temperature/heat flux model. The LSM algorithm is used to get the optimal solution. Figure 5 illustrates the measured TEM heat flux compared with the estimated one by the identified model with $n=m=3$. The obtained results show good approximations of the real heat flux based on the previous measurement of the temperature. In the worst case, the error between the real and estimated heat fluxes reached 0.0025 W. The estimated parameters are given in Ref. [32].

4 Thermal Teleoperator Modeling

In the human operator side of the telepresence system, the TEM is used as a thermal display to replicate, on the operator's finger, the thermal exchange occurring at the remote side. The thermal display is controlled according to the estimated temperature and the heat flux of the remote probed object (by the thermal robotic finger). In the remote side of the telepresence, the TEM is used to replicate the thermal interaction occurring between the operator's finger pad and the display: In simple words, it will act as a thermal source behaving thermally as the human finger pad; it is driven according to the estimated temperature and the heat flux occurring at the operator finger, as shown in Fig. 6. In this way, we ensure a bilateral control between the master and the slave sites that reproduces in a most transparent and stable way the thermal sensations experienced in both sides.

4.1 Basic Thermal Transfer Equations. When two objects of different materials with different initial temperatures T_{1i} and T_{2i}, respectively, are placed in contact, Fig. 7, thermal conduction is the dominant mode of heat transfer and convection can be neglected [8]. Fourier's law of heat conduction relates the heat transfer rate to the temperature gradient as follows [33]:

$$\frac{\partial T_1(x,t)}{\partial t} = \alpha_1 \frac{\partial^2 T_1(x,t)}{\partial x^2} \tag{18}$$

$$\frac{\partial T_2(x,t)}{\partial t} = \alpha_2 \frac{\partial^2 T_2(x,t)}{\partial x^2} \tag{19}$$

where the indices 1 and 2 state for materials 1 and 2, respectively, and α_1 and α_2 are the thermal diffusivities.

The initial conditions are

$$T_1(0,t) = T_{1i} \tag{20}$$

$$T_2(0,t) = T_{2i} \tag{21}$$

and the boundary conditions are

$$k_1 \frac{\partial T_1(0,t)}{\partial x} = k_2 \frac{\partial T_2(0,t)}{\partial x} \tag{22}$$

$$T_1(0,t) = T_2(0,t) \tag{23}$$

where k_1 and k_2 are the thermal conductivities.

The sensor has a thickness $e=0.42$ mm. Because of its small thickness, thermal transfer within the sensor section may be assumed to be linear and homogeneous. The quantity of the heat transferred between the two materials in contact is defined by

$$Q(x,t) = -k \times \nabla T = -kS \frac{\partial T(x,t)}{\partial x} \tag{24}$$

where Q is the quantity of heat, S denotes the surface of the contact area, and k denotes the sensor conductivity.

The heat transferred will increase the temperature of the colder

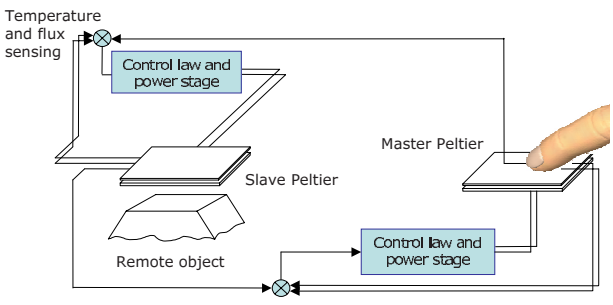

Fig. 6 Overview of the thermal telepresence control scheme

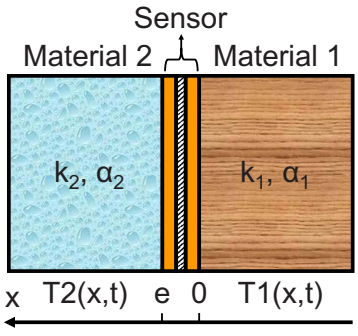

Fig. 7 Thermal contact modeling

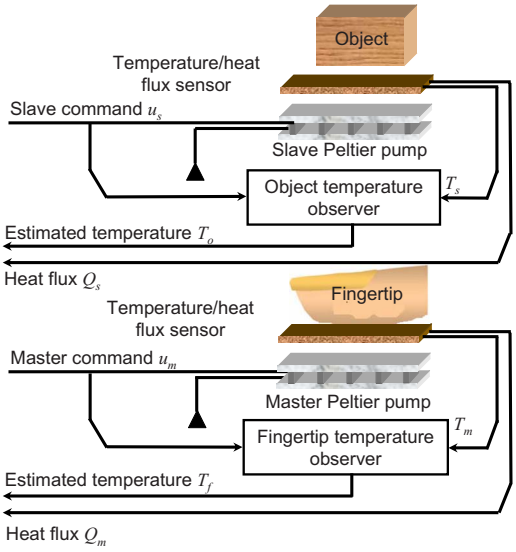

Fig. 8 Temperature estimation scheme

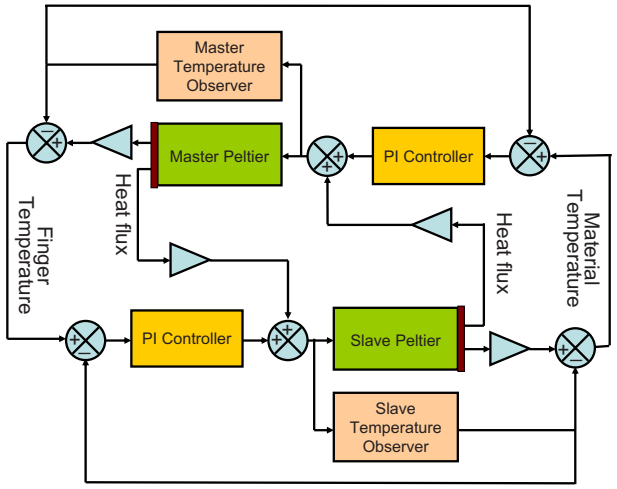

Fig. 9 Overall bilateral controller of the thermal telepresence

material and decrease that of the warmer material. The heat transfer at the limit of the contact area is equal along the x axis, $Q(x,t)=Q(x+\Delta x,t)$, and the temperature equation becomes [24]

$$\alpha\frac{\partial^2 T(x,t)}{\partial x^2}=0 \tag{25}$$

Thermal contact resistance is ignored since thermal grease is used at the contact surface of the TEM and also the surface of the objects is smoothened.

One general solution is $T(x)=c_1x+c_2$; with the limit conditions $T_{x=0}=T_1$ and $T_{x=e}=T_2$, where e is the contact area thickness, we have

$$T(x)=T_1-\frac{x}{e}(T_1-T_2) \tag{26}$$

A linear and homogeneous temperature profile across the sensor section allows determining the temperature evolution of any point being at a distance x within the sensor according to Eq. (26), see Fig. 7. Since the thermocouple is embedded at the center of the sensor ($x=e/2$) between two conductive plates made of copper, the temperature evolution is then

$$T_{e/2}=(T_1+T_2)/2 \tag{27}$$

Then,

$$T_2=2T(e/2)-T_1 \tag{28}$$

From Eq. (24), the heat flux evolution is

$$Q=\frac{kS(T_1-T_2)}{e}=\frac{(T_1-T_2)}{e/kS} \tag{29}$$

Making analogy with Ohm's law in electricity, the difference (T_1-T_2) between two given points in each side creates a temperature flux Q between these two points. This is equivalent to an electrical potential difference applied to the two ends of a resistance. We call thermal resistance R_{th} the quantity e/kS. Under the influence of the temperature difference (T_1-T_2), the heat flux increases the temperature of the cold points in the contact area trying to reach equilibrium.

4.2 Finger and Object Temperature Estimation. Figure 8 represents the proposed estimation scheme for the thermal telepresence. Based on Eq. (28), the object/fingertip temperature observers compute the estimated object/fingertip temperature as follows:

$$T^{(f)}=2T^{(m)}-T_p^{(m)} \tag{30}$$

$$T^{(o)}=2T^{(s)}-T_p^{(s)} \tag{31}$$

The variables $T^{(m,s)}$ denote the sensor temperature output and $T_p^{(m,s)}$ denote the estimated temperature of the TEMs computed using the identified models in Eq. (10):

$$T_p^{(m,s)}(t)=-\sum_{i=1}^{3}\sum_{k=0}^{3}a_{ik}u^{(m,s)}(t-i)^kT^{(m,s)}(t-i)+\sum_{j=1}^{3}\sum_{h=0}^{3}b_{jh}u^{(m,s)}(t-j)^hu^{(m,s)}(t-j) \tag{32}$$

where $u^{(m,s)}$ denote the commands (input currents) and $T^{(f,o)}$ denote the temperature evolutions observed for both operator's fingertip (f) and remote manipulated object (o).

5 Bilateral Controller Implementation

5.1 Temperature Control. A typical TEM temperature controller uses a PID controller. Although useful, it suffers from a dependence on the ambient temperature condition. The differential term attempts to measure the heating/cooling rate of the TEM to overcome this problem; but being a derivative, it is inherently unstable for fast temperature variation as is the case with an abrupt contact. The heat flux sensor used offers an elegant alternative to the differential term because it measures directly the heating/cooling rate in the TEM and does not depend on the thermal ambient conditions and perturbations.

A PID controller using the heat flux sensor gets the derivative term with the sensor output as follows:

$$u(t)=k_pe(t)+k_i\int_0^t e(\tau)d\tau+k_QQ \tag{33}$$

where k_p and k_i are, respectively, the proportional and integral gains, $e(t)$ is the temperature error, Q is the heat flux, and k_Q is the heat flux factor. The use of the heat flux term effectively predicts where the temperature is going and allows a feed-forward control of the Peltier device as in Ref. [34].

5.2 Bilateral Temperature Control. In Ref. [11], the controller used is based on bilateral coupling between the heat flux and the temperature variables and is implemented using a stable four channel architecture. In the present work, we use a temperature/temperature bilateral coupling between the master and the slave with heat flux feed-forward control as described above. Figure 9

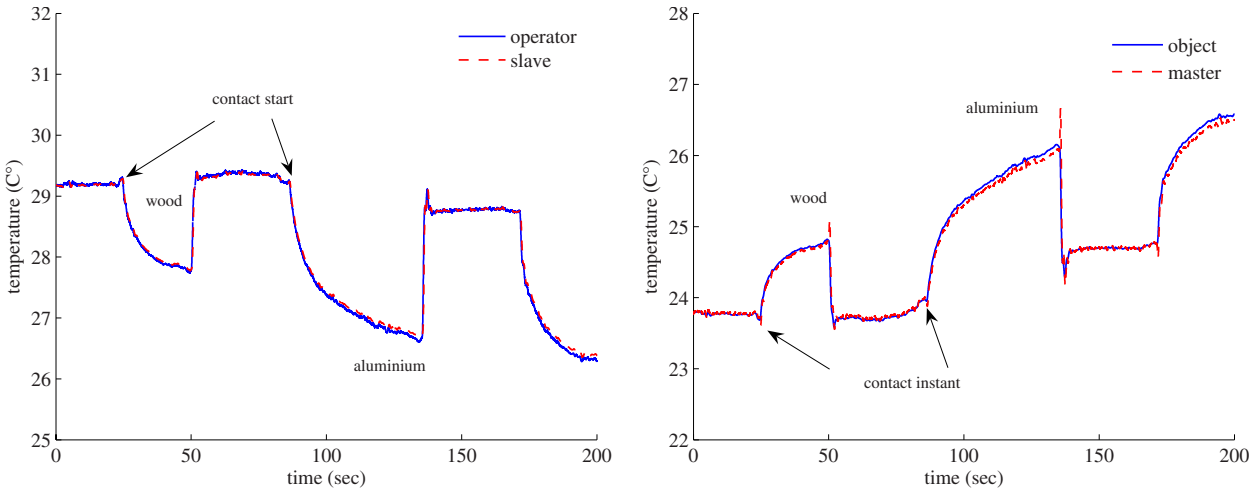

Fig. 10 Remote robotic finger Peltier temperature controlled with the estimated finger temperature during consecutive contact (left). Thermal display Peltier temperature controlled with the estimated temperature of touched objects (right).

shows a general view of the bilateral controller.

The control laws for both the master (m) and the slave (s) are defined, in the Laplace domain, as follows:

$$u^{(m)} = \left\{ k_p^{(m)} + \frac{k_i^{(m)}}{s} \right\} (T^{(o)} - T_p^{(m)}) + k_Q^{(m)} Q^{(s)} \tag{34}$$

$$u^{(s)} = \left\{ k_p^{(s)} + \frac{k_i^{(s)}}{s} \right\} (T^{(f)} - T_p^{(s)}) + k_Q^{(s)} Q^{(m)} \tag{35}$$

where $u^{(m,s)}$ denote the commands (input currents), $Q^{(m,s)}$ are the measured heat fluxes, and $k_p^{(m,s)}$, $k_i^{(m,s)}$, and $k_Q^{(m,s)}$ are the proportional, integral, and feed-forward gain factors, respectively.

5.3 Experimental Results and Discussion. For thermal feedback experiments, objects made of aluminum, steel, and wood are used as remote objects in contact with the slave part. The surface of the objects is smoothened to reduce roughness and ensure a minimal thermal contact resistance with a constant pressure force. In our experiments, the operator's finger is always touching the thermal display pad, whereas the remote probing thermal pad repeats touch-and-release to/from remote objects.

While the slave device is not in contact with any object, the estimated temperature using Eq. (31) is influenced by both the ambient air (air convection) and the master device since the slave device is controlled to track the temperature of the finger in a bilateral way. Therefore, the estimated temperature will be somewhat greater than that of the ambient air.

The experimental curves in the case of contact with wood and aluminum blocks are shown in Fig. 10. The proposed method gives good tracking performances of temperature exchanges. The operator is more sensitive to temperature drop and heat flux changes occurring in remotely probing an object, namely, at first contacts. Note that the same experimental object temperature is reproduced under the operator finger, which leads to good thermal sensations.

Materials with large thermal conductivity are found to be easier to discriminate compared with objects having smaller thermal conductivity, especially in the case of consecutive contact (small or no thermal adaptation of the finger) and this demonstrates a satisfactory accordance as in the case of consecutive contact with real objects [35,36]. Materials with relatively similar heat conductivity such as wood and polyvinyl chloride are difficult to distinguish. This is due, from our first trials, to imperfect contact conditions.

The fact that the thermal display reproduces the probed material thermal exchange behavior and the probe thermal device reproduces the finger thermal behavior improves the quality of thermal interaction transparency so that it improves the perceptual realism in telepresence. The advantage of our approach is that it does not require knowledge about the thermal properties of the finger nor the material. However, it only works in a telepresence context in which real materials are present at the slave side, not in a pure virtual environment.

In addition, the temperature estimation is altered by the presence of metabolic processes (human finger) and thermal inertia of the sensors that affects the time response of the thermal displays used in this experiments, so future models should get ride of these factors.

6 Conclusion

In this work, we proposed three models describing thermoelectric module performance in steady-state and transient phases. The proposed models have been identified using the LSM and RLSM algorithms and assessed experimentally. They allow the analysis of TEM heat flux and temperature behavior using linear and nonlinear recursive ARMA equations. Using the identified models of the TEMs, we present a new approach for thermal feedback based on the material and finger temperature estimation with heat flux feed-forward control. The rendering scheme uses a bilateral coupling law to reproduce the operator and the remote material's thermal interaction in order to ensure realistic thermal sensation.

We expect that the proposed thermal feedback will contribute to the generation of more realistic haptic sensation that will increase the quality of operator telepresence in real or virtual environments. In other applications, thermal feedback could be used as a sensory substitute or adjunct for visual and/or tactile feedback. Although the obtained results are satisfactory for thermal rendering, some issues must be investigated further, namely, (i) designing an artificial probing finger with materials having thermal and mechanical properties as close as possible to that of the human finger, (ii) designing closed-loop controllers based on thermal impedance shaping scheme, and (iii) using faster response and less inertia temperature/flux sensors.

Acknowledgment

Thanks to Abdelhamid Drif for helping in the preliminary design of the thermal setup.

Nomenclature

T_h = temperature of the hot side of the pump

T_c = temperature of the cold side of the pump
π = Peltier coefficient
α_s = Seebeck coefficient
T = absolute temperature
I = electric current
τ = Thomson coefficient
x = space variable
t = time variable
E = energy
P_p = quantity of heat liberated due to the Peltier effect
P_t = quantity of heat liberated due to the Thomson effect
P_j = quantity of heat liberated due to the Joule effect
P_k = quantity of heat liberated due to the conduction effect
P_c = cooling capacity of the pump
P_h = heating capacity of the pump
a_i, b_j = temperature model parameters
n, m = model's order according to T
p, q = polynome order according to a and b
θ = vector of parameters
φ = regression vector of dimension d
Q = heat flux
c_i, d_j = heat flux model parameters
$\Phi_{h,c}$ = measurement matrices
T_{1i}, T_{2i} = initial temperatures
α_i = thermal diffusivity
k_i = thermal conductivity
e = sensor thickness
Q = quantity of heat
S = surface of the contact area
R_{th} = thermal resistance
$T^{(o,f)}$ = estimated object (o)/fingertip (f) temperature
$T^{(m,s)}$ = sensor temperature output
$T^{(m,s)}$ = estimated temperature of the TEMs
$u^{p}_{(m,s)}$ = commands (input currents)
k_p, k_i = proportional and integral gains
$e(t)$ = temperature error
k_Q = heat flux factor
K = Kalman gain update

References

[1] Jones, L. A., and Ho, H.-N., 2008, "Warm or Cool, Large or Small? The Challenge of Thermal Displays," IEEE Transactions on Haptics, **1**(1), pp. 53–70.
[2] Russell, R. A., 1988, "Thermal Sensor for Object Shape and Material Constitution," Robotica, **6**(01), pp. 31–34.
[3] Caldwell, D. G., Andersen, U., Bowler, C., and Wardle, A., 1995, "A High Power Weight Dexterous Manipulator Using Sensory Glove Based Motion Control and Tactile Feedback," Trans. Inst. Meas. Control (London), **17**(5), pp. 234–241.
[4] Ottensmeyer, M., and Salisbury, J., 1997, "Hot and Cold Running VR, Adding Thermal Stimuli to Haptic Experience," Proceedings of the PHANToM Users Group.
[5] Benali-Khoudja, M., Hafez, M., Alexandre, J. M., Benachour, J., and Kheddar, A., 2003, "Thermal Feedback Model for Virtual Reality," International Symposium on Micromechatronics and Human Science, pp. 153–158.
[6] Yamamoto, A., Cros, B., Hashimoto, H., and Higuchi, T., 2004, "Control of Thermal Tactile Display Based on Prediction of Contact Temperature," IEEE International Conference on Robotics and Automation.
[7] Deml, B., Mihalyi, A., and Hannig, G., 2006, "Development and Experimental Evaluation of a Thermal Display," EuroHaptics, pp. 257–262.
[8] Ho, H.-N., and Jones, L. A., 2006, "Thermal Model for Hand-Object Interactions," Symposium on Haptic Interfaces for Virtual Environments and Teleoperator Systems, pp. 461–467.
[9] Ho, H.-N., and Jones, L. A., 2007, "Infrared Thermal Measurement System for Evaluating Model-Based Thermal Displays," *WHC'07: Proceedings of the Second Joint EuroHaptics Conference and Symposium on Haptic Interfaces for Virtual Environment and Teleoperator Systems*, IEEE Computer Society, Washington, DC, pp. 157–163.
[10] Sarda, A., Deterre, R., and Vergneault, C., 2004, "Heat Perception Measurements of the Different Parts Found in a Car Passenger Compartment," Measurement, **35**, pp. 65–75.
[11] Drif, A., Citérin, J., and Kheddar, A., 2005, "Thermal Bilateral Coupling in Teleoperators," IEEE/RSJ International Conference on Robots and Intelligent Systems, pp. 1301–1306.
[12] Guiatni, M., Benallegue, A., and Kheddar, A., 2008, "Learning-Based Thermal Rendering for Telepresence," *Proceedings of the 6th International Conference on Haptics: Perception, Devices and Scenarios*, EuroHaptics '08, Madrid, Spain, Springer-Verlag, Berlin, Heidelberg, pp. 820–825.
[13] Guiatni, M., Benallegue, A., and Kheddar, A., 2009, "Thermal Display for Telepresence Based on Neural Identification and Heat Flux Control," Presence: Teleoperators and Virtual Environments, MIT Press, **18**(2), pp. 156–169.
[14] Ciccarella, G., and Marletti, P., 1989, "Model Reference Adaptive Control of a Thermostatic Chamber," IEEE Trans. Ind. Electron., **36**(1), pp. 88–93.
[15] Schutze, J., Ilgen, H., and Fahrner, W. R., 2001, "An Integrated Micro Cooling System for Electronic Circuits," IEEE Trans. Ind. Electron., **48**(2), pp. 281–285.
[16] Hodes, M., 2007, "Optimal Pellet Geometries for Thermoelectric Refrigeration," IEEE Trans. Compon. Packag. Technol., **30**(1), pp. 50–58.
[17] Solbrekken, G. L., Yazawa, K., and Bar-Cohen, A., 2008, "Heat Driven Cooling of Portable Electronics Using Thermoelectric Technology," IEEE Trans. Adv. Packag., **31**(2), pp. 429–437.
[18] Citérin, J., Pocheville, A., and Kheddar, A., 2006, "A Touch Rendering Device in a Virtual Environment With Kinesthetic and Thermal Feedback," IEEE International Conference in Robotics and Automation, pp. 3923–3928.
[19] Lau, P., and Buist, R., 1996. "Temperature and Time Dependent Finite Difference Model of a Thermoelectric Pellet and Couple," International Conference on Thermoelectrics, pp. 227–233.
[20] Helmers, L., Müller, E., Schilz, J., and Kaysser, W. A., 1998, "Graded and Stacked Thermoelectric Generators—Numerical Description and Maximization of Output Power Mater," Mater. Sci. Eng., B, **56**(1), pp. 60–68.
[21] Seifert, W., Ueltzen, M., Strumpel, C., Heiliger, W., and Muller, E., 2001, "One-Dimensional Modeling of a Peltier Element," International Conference on Thermoelectrics, pp. 439–443.
[22] Lineykin, S., and Ben-Yaakov, S., 2007, "Modeling and Analysis of Thermoelectric Modules," IEEE Trans. Ind. Appl., **43**(2), pp. 505–512.
[23] Neto, A., de-Almeida, L., Lima, A., and Deep, G., 2003, "Recursive ARMA Modeling for Thermoelectric Modules," 20th IEEE Instrumentation and Measurement Technology Conference (IMTC'03), pp. 919–923.
[24] Carslaw, H. S., and Jaeger, J. C., 1959, *Conduction of Heat in Solids*, Clarendon Press, Oxford.
[25] Labudovic, M., and Li, J., 2004, "Modeling of Thermoelectric Cooling of Pump Lasers," IEEE Trans. Compon. Packag. Technol., **27**, pp. 724–730.
[26] Chen, J., Yan, Z., and Wu, L., 1997, "Nonequilibrium Thermodynamic Analysis of a Thermoelectric Device," Energy, **22**(10), pp. 979–985.
[27] Hodes, M., 2005, "On One-Dimensional Analysis of Thermoelectric Modules (TEMs)," IEEE Trans. Compon. Packag. Technol., **28**(2), pp. 218–229.
[28] Martorana, R. T., 1975, "Thermoelectric Temperature Control of Instrumentation—A Sample Design," IEEE Trans. Ind. Electron. Control Instrum., **IECI-22**(1), pp. 69–75.
[29] Mitrani, D., Tome, J. A., Salazar, J., Turo, A., Garcia, M. J., and Chavez, J. A., 2005, "Methodology for Extracting Thermoelectric Module Parameters," IEEE Trans. Instrum. Meas., **54**(4), pp. 1548–1552.
[30] Harvey, R. D., Walker, D. G., and Frampton, K. D., 2007, "Enhancing Performance of Thermoelectric Coolers Through the Application of Distributed Control," IEEE Trans. Compon. Packag. Technol., **30**(2), pp. 330–336.
[31] Beaudoin, P. M., Audet, Y., and Bendali, A., 2008, "Characterizing a Thermoelectric Module as Part of a Semiconductor Course Laboratory," IEEE Trans. Educ., **51**(2), pp. 282–287.
[32] Guiatni, M., Drif, A., and Kheddar, A., 2007, "Thermoelectric Modules: Recursive Nonlinear ARMA Modeling, Identification and Robust Control," 33rd Annual Conference of the IEEE Industrial Electronics Society (IECON), pp. 568–573.
[33] Incropera, F., DeWitt, D., Bergman, T., and Lavine, A., 2006, *Fundamentals of Heat and Mass Transfer*, 6th ed., Wiley, New York.
[34] Lartz, D. J., Cudney, H. H., and Diller, T. E., 1994. "Heat Flux Measurement Used for Feedforward Temperature Control," Tenth International Heat Transfer Conference, pp. 261–266.
[35] Dyck, P. J., Curtis, D. J., Bushek, W., and Offord, K., 1974, "Description of 'Minnesota Thermal Disks' and Normal Values of Cutaneous Thermal Discrimination in Man," Neurology, **24**, pp. 325–330.
[36] Ho, H.-N., and Jones, L. A., 2006, "Contribution of Thermal Cues to Material Discrimination and Localization," Percept. Psychophys., **68**(1), pp. 118–128.